Fisheries Research 268 (2023) 106856

Contents lists available at ScienceDirect

Fisheries Research

journal homepage: www.elsevier.com/locate/fishres

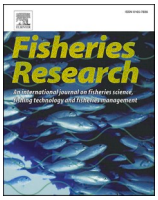

How to obtain clear images from in-trawl cameras near the seabed? A case study from the Barents Sea demersal fishing grounds

Maria Tenningen [a,*], Shale Rosen [a], E.H. Taraneh Westergerling [a,b,1], Nils Olav Handegard [a]

[a] Institute of Marine Research, P.O box 1870 Nordnes, 5817 Bergen, Norway
[b] University of Bergen, Department of Biology, Thormøhlensgate 53 A/B, 5006 Bergen, Norway

ARTICLE INFO

Handled by B. Morales-Nin

Keywords:
Trawl camera
Underwater camera
Deep Vision
Demersal trawl
Sediment plume

ABSTRACT

Underwater camera systems are commonly used for monitoring fish and fishing gear behaviours. More recently, camera systems have been applied to scientific trawl surveys for improved spatial resolution and less invasive sampling and to commercial fisheries for better catch control and reduced by-catch. A challenge when using cameras in demersal trawls is poor image clarity due to the door and ground gear generated sediment plume. In this study we have measured the height of the sediment plume produced by a large commercial trawl in the Barents Sea using acoustic methods and investigated its effect on in-trawl camera image clarity. The trawl extension was lengthened, and additional buoyancy added to lift the camera system in the aft end of the trawl. The camera system was tested at increasing heights above seabed until no sediment plume was visible in the images. Based on the acoustic data the sediment plume was measured to be on average 4–5 m (SD 1.7 m) above sea floor. Image clarity improved significantly as the camera system clearance from seabed increased from 4 to 11 m. No effect of sediment type on image clarity was identified. The trawl modifications did not affect the trawl's opening geometry or bottom contact. However, the increased length and angle of the under panel aft in the trawl and in the extension appears to have resulted in reduced water flow and may influence the passage and retention of fish. The feasibility of using camera systems in demersal trawls and this and other solutions for obtaining clear images are discussed.

1. Introduction

Underwater cameras attached to trawls have commonly been used for studying fish behaviour in fishing gears since the 1960 s and have become essential tools when testing gear modifications for improved fishing efficiency and selectivity (Graham et al., 2004; Urquhart and Stewart, 1993; Winger et al., 2010). More recently, in-trawl stereo camera systems have been used to obtain quantitative data on fish size, densities and behaviour in the trawl (Boldt et al., 2018; Graham et al., 2004; Rosen and Holst, 2013; Williams et al., 2013).

In scientific trawl surveys image data can be used for improved spatial and taxonomic resolution and less invasive sampling. A wider range of species compared to conventional sampling can be monitored. This is useful information when moving from single species surveys to surveys covering a wider range of the trophic levels. They can, for example, provide information about small and sensitive organisms that are not retained in the codends of traditional fish sampling trawls (Underwood et al., 2014; Allken et al., 2021) and sample multiple depths in the pelagic zone during a single trawl haul (Rosen and Holst, 2013). The latter being particularly useful for acoustic target classification for acoustic-trawl surveys.

Despite advantages over traditional trawling, video-trawling is currently only used in few scientific surveys as a standard method. It is being considered for the acoustic and trawl survey for New England groundfish (DeCelles et al., 2017; Stokesbury et al., 2017). In this survey trawling is conducted with open codend, fish are identified and counted as they pass the camera and are then released at the fishing depth after being imaged. This allows for long transects, making the sampling more efficient and sustainable. Short hauls with the codend closed are made to obtain biological samples. An open codend trawl with an underwater camera system has also been used in estuary surveys for identification and counting small and sensitive organisms (Feyrer et al., 2013). Image-based technologies are more commonly used to assess benthic species. As an example, Norway lobster (*Nephrops norvegicus)* stock

* Corresponding author.
E-mail address: maria.tenningen@hi.no (M. Tenningen).
[1] https://orcid.org/0000-0001-6990-3775

https://doi.org/10.1016/j.fishres.2023.106856
Received 20 December 2022; Received in revised form 24 August 2023; Accepted 13 September 2023
Available online 20 September 2023

abundance is based on surveys where a video camera is mounted on a towed sledge. Burrows are then identified in the footage and their density used as an index of abundance (ICES, 2017). For this survey it is also being considered to attach cameras to trawls to combine stock monitoring with fishing operations for more efficient data collection including by-catch monitoring (Fonseca et al., 2008).

Camera systems are also becoming available for commercial fisheries. Live video feeds help identify areas with good availability of target species or high number of by-catch species. Fishers can then choose to either stay in the area or move to another area based on what is entering the trawl. In the trawl fisheries for Alaska pollock (*Gadus chalcogrammus*) and Pacific hake (*Merluccius productus*), in-trawl cameras are used to identify by-catches of salmon (*Onchorhynchus spp.*) and rockfish (*Sebastes spp.*) (Rose and Barbee, 2022). A camera system is currently being developed for the Norway lobster fishery (Sokolova et al., 2021b, 2022). In the future it is also likely that the fisher can, based on image information, decide whether to catch or retain the fish by opening or closing the codend (Rose and Barbee, 2022).

One of the main challenges with in-trawl camera systems is the large amount of image data that need to be processed. However, automatic machine learning based methods are becoming increasingly available, and algorithms to automatically identify, count, and length measure individuals by species are being developed. Such systems are now available for counting and identifying pelagic species (Allken et al., 2021, 2019; Garcia et al., 2020) and *Nephrops* in demersal trawls (Sokolova et al., 2021a). Similar machine-learning based systems have also been developed for video surveys conducted from towed sleds (Naseer et al., 2022) and freshwater applications, including fish passages (Bravata et al., 2020).

Another challenge when using camera systems in demersal trawls is poor image clarity due to sediment mobilization by the trawl doors and ground gear (DeCelles et al., 2017; Fonseca et al., 2008; Sokolova et al., 2022). The sediment plume has an important role in herding and capturing demersal species (Kim and Wardle, 1998) and removing it by lifting the doors or ground gear above seabed has been shown to result in reduced catch rates (Sistiaga et al., 2015). The density, height and endurance of the sediment plume depend on the type of seabed, the type of trawl and trawling speed (O'Neill and Summerbell, 2011). Image clarity is therefore likely to vary depending on fishing method and area.

The Barents Sea demersal fisheries target mainly cod (*Gadus morhua*), haddock (*Melanogrammus aeglefinus*) and saithe (*Pollacius virens*). The stocks are managed with individual vessel quotas and minimum landing sizes combined with real-time closures, a discard ban, and technical measures for size selectivity. Rigid sorting grids in combination with diamond mesh codends have been mandatory in the Barents Sea demersal cod and haddock fishery since 1997 (Grimaldo et al., 2014; Gullestad et al., 2015). Since larger fish generally command a higher price and fishing grounds get closed when the proportion of bycatch or undersized individuals is high, fishers have a financial incentive to fish selectively. Excessive catches that exceed processing capacity, result in reduced fish quality or net damage have also been a problem in recent years as a results of increasing stock sizes (Grimaldo et al., 2018, 2014). A camera system in the trawl for identification of catch density, species and size compositions could potentially improve selectivity and catch control in these fisheries.

The Deep Vision camera system produced by Scantrol DV AS (Rosen and Holst, 2013) was used in a demersal survey trawl in November 2018 in the Barents Sea. However, the trials were suspended after just three trawl hauls as large quantities of suspended sediment, rocks and gravel entered the system, risking damage and severely limiting the usability of the images (Shale Rosen, unpublished data). The objective of the present study was to first measure the height of the sediment plume created by the ground gear of a large commercial trawl typical to the demersal fishery in the Barents Sea using acoustic methods. Second, to investigate the effect of the sediment plume on in-trawl camera image clarity. Third, to develop and evaluate a method to obtain clear images by raising the trawl extension with the camera system attached above the sediment plume. Two camera systems were used in this study, a Go Pro camera was used in the first trawl hauls where different trawl configurations were evaluated and the Deep Vision camera system once it was considered safe to attach the system in the trawl.

2. Materials and methods

2.1. Study time and area

The data presented in this study were collected in November 2021 in the traditional demersal fishing grounds in the Barents Sea off the north coast of Norway (Fig. 1). The experiments were conducted on board the 77.5 m long, 4067 gross register tonnage R/V "G.O. Sars" (IMO number 9260316).

Water depth in the study area varied between 75 and 390 m (Table 1). Seabed sediment type was not sampled in this study but has been previously mapped and published by the Geological Survey of Norway and the MAREANO project (Bøe et al., 2022). The seabed is mapped by multibeam echosounder surveys combined with predetermined stations (about 10 stations per 1000 km^2) where video data are collected for visual determination of seabed sediments. In some of these stations (approximately 2 per 1000 km^2) physical sediment samples are also collected. Detailed information about sediment type for the areas where trawling was conducted in this study are presented in Table 1.

2.2. Trawl experiments and instrumentation

In total 24 hauls using a Selstad Streamline 630 demersal trawl were made during the survey (Table 1, Fig. 2). The trawl had 170 mm mesh in the wings and forepart and 155 mm mesh in the belly and aft sections. The total stretched length from the center of the footrope to the end of the trawl was 75 m. The trawl was outfitted with a 30.5 m long ground gear with 600 mm rubber rockhopper disks and spread using 8 m^2

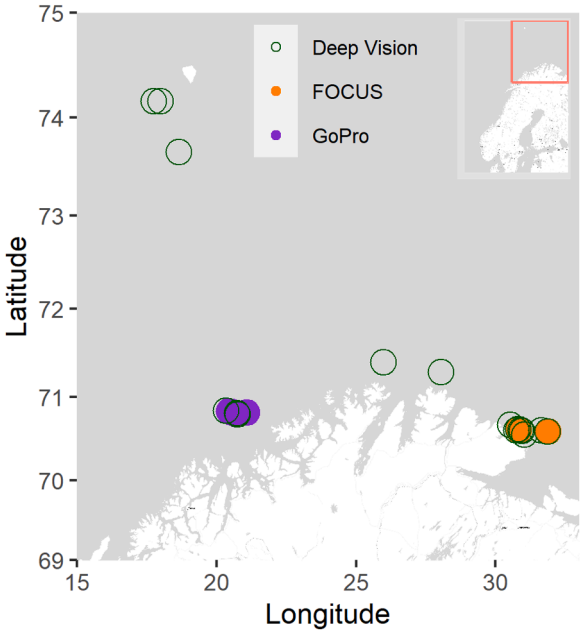

Fig. 1. Survey area off the northern coast of Norway in the Barents Sea. Symbol shape and colour indicate whether a GoPro or Deep Vision camera system was used for image analyses and the locations where the FOCUS underwater vehicle was used for acoustic measurements of sediment plume height. The small map of Norway, Sweden and Finland in the top right corner indicates the sampling area with the red rectangle.

Table 1
Summary of trawl hauls. Including modifications made to the trawl extension, numbers of GoPro and Deep vision images analysed for clarity and hauls where the underwater vehicle (FOCUS) was used either for measurements of trawl geometry or sediment plume height with acoustics.

Haul No	Date (yyyy-mm-dd)	Start Lat (N)	Start Lon (E)	Tow time (min)	Bottom depth (m)	Sediment type	Extension modification (length of additional extension and number of floats)	Codend clearance (m)	Go Pro images (No)	Deep Vision images (No)	FOCUS data collected
1	2021–11–02	70.81	20.66	21	230	Muddy sand	10.7 m diamond mesh; 0 floats	3.6[a]	118	0	
2	2021–11–02	70.82	20.56	148	230	Sandy mud	10.7 m diamond mesh; 0 floats	3.9 (0.6)	738	0	Geometry
3	2021–11–03	70.83	20.45	102	230	Gravelly muddy sand	15 m square mesh; 0 floats	4.3 (0.6)	608	0	Geometry
4	2021–11–03	70.80	20.72	105	230	Muddy sand	15 m square mesh; 22 floats	6.2 (0.4)	630	0	Geometry
5	2021–11–03	70.82	20.61	98	220	Muddy sand	15 m square and 22 m diamond mesh; 44 floats	10.9 (1.5)	423	0	Geometry
6	2021–11–04	70.80	20.75	97	230	Muddy sand	15 m square and 22 m diamond mesh; 44 floats	10.4 (0.3)	0	100	Geometry
7	2021–11–04	70.84	20.33	98	230	Muddy sand	22 m diamond mesh; 30 floats	6.0[a])	0	100	Geometry
8	2021–11–05	70.81	20.73	91	220	Muddy sand	22 m diamond mesh; 44 floats	9.4 (1.1)	0	100	Geometry
9	2021–11–07	71.40	25.97	117	260	Gravelly sand	22 m diamond mesh; 44 floats	9.6 (0.5)	0	100	Geometry
10	2021–11–07	71.29	28.04	31	390	Gravelly sand	22 m diamond mesh; 44 floats	10.5 (0.5)	0	100	
11	2021–11–08	70.67	30.51	8	75	Sandy gravel	22 m diamond mesh; 44 floats	9.6[b]	0	100	
12	2021–11–08	70.61	30.82	31	170	Gravelly sand	22 m diamond mesh; 44 floats	9.6[b]	0	100	
13	2021–11–12	73.66	18.65	29	320	Muddy sandy gravel	22 m diamond mesh; 44 floats	9.4 (0.7)	0	100	
14	2021–11–13	74.16	17.75	23	190	Muddy sandy gravel	22 m diamond mesh; 44 floats	9.4 (0.7)	0	100	
15	2021–11–13	74.16	17.99	81	130	Muddy sandy gravel	22 m diamond mesh; 44 floats	9.5 (0.5)	0	0	Acoustic
16	2021–11–15	70.61	30.82	34	140	Sand gravel and cobbles	22 m diamond mesh; 44 floats	9.2 (1.2)	0	100	
17	2021–11–15	70.62	30.8	26	170	Sandy gravel	22 m diamond mesh; 44 floats	9.4 (0.5)	0	100	
18	2021–11–15	70.60	30.94	46	170	Sandy gravel	22 m diamond mesh; 44 floats	9.6[b]	0	100	
19	2021–11–16	70.61	30.89	30	170	Gravelly sand	22 m diamond mesh; 44 floats	9.2 (0.5)	0	100	
20	2021–11–16	70.61	30.74	33	140	Sand, gravel, cobbles and boulders	22 m diamond mesh; 44 floats	9.7 (0.3)	0	100	
21	2021–11–16	70.56	31.02	33	130	Gravelly muddy sand	22 m diamond mesh; 44 floats	9.5 (1.1)	0	100	
22	2021–11–16	70.61	31.64	30	280	Gravelly sandy mud	22 m diamond mesh; 44 floats	9.4 (0.8)	0	100	
23	2021–11–17	70.59	31.88	83	250	Gravelly muddy sand	22 m diamond mesh; 44 floats	9.7 (0.2)	0	0	Acoustic
24	2021–11–17	70.59	31.86	31	250	Gravelly muddy sand	22 m diamond mesh; 44 floats	10.3 (1.3)	0	100	

[a] Average height above seabed was measured with the scanning sonar on the FOCUS vehicle
[b] Height data was not available and the value is based on the average height in hauls with the same trawl rigging.

Thyborøn 23 VFG trawl doors. The sweeps (cables between doors and headline / ground gear) were 50 m long. A 10.7 m long transition section was attached to the back of the trawl to connect the 2-panel trawl to 4-panel experimental extensions. The transition section was constructed of 155 mm diamond mesh. The upper and lower panels were tapered 4 N – 5B and side panels 3 N – 1B, ending up in 4 panels with 24 meshes in each side. A 12 m long codend with 24 mm mesh size (much smaller mesh than in a commercial trawl codend) was used to ensure that all fish passing through the Deep Vision camera system were caught for other unrelated studies carried out simultaneously.

In the first 8 hauls rigging tests were conducted to get a general idea of water clarity and the height of the sediment plume. Different combinations of diamond and square mesh extensions (155 mm mesh, 8 mm diameter twine) and additional floats were attached behind the 2–4 panel transition to test and identify the best option for raising the camera system above the sediment plume (Table 1). A stone release was attached straight ahead of the 2–4 panel transition piece to avoid stones entering the delicate Deep Vision stereo camera system. The stone release was created by removing a 1 m wide triangle from the under panel of the trawl. The underside was covered with a mat with short hanging ropes to prevent fish from escaping ("chafing gear"). These test hauls were made off the north-western coast of Norway at water depths of 220 – 230 m (Fig. 1). The seabed sediment in this area was a mixture of mud, sand and gravel (Table 1). In the first five trawl hauls, GoPro video cameras (GoPro HERO 3 + silver) with light source (2 ×1050 lumen white Brinyte DIV01) were attached in the upper panel about 2 m from the end of the extension sections, facing forward (Fig. 2).

The subsequent 17 trawl hauls (excluding hauls 15 and 23, where a new Deep Vision system for the commercial fisheries not part of this study was tested) were conducted with the Deep Vision system (Table 1).

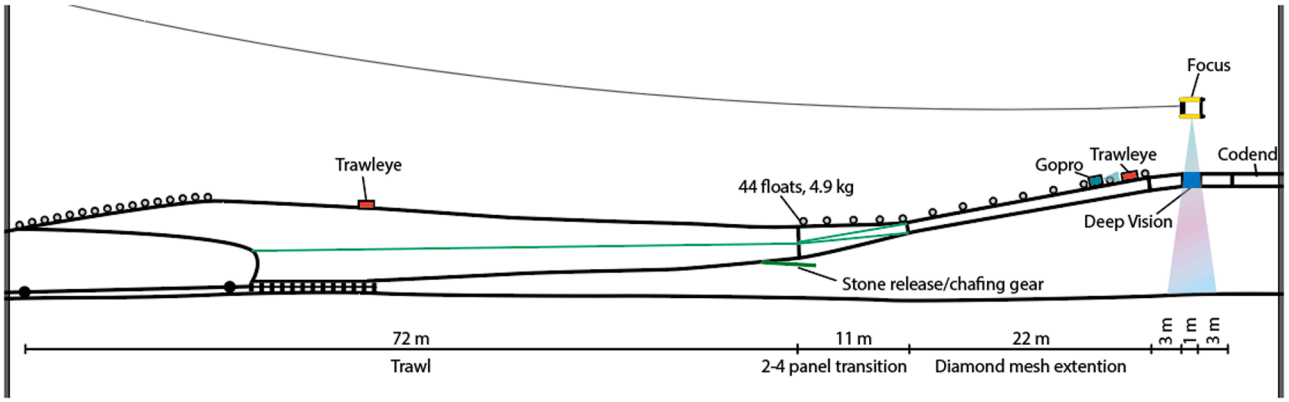

Fig. 2. Illustration of the Selstad Streamline 630 trawl with modified extension to raise Deep Vision camera system above seabed and the main monitoring instruments (side view). The green line illustrates net panel seams in the 2-panel trawl and 2–4 panel transition section.

These trawl hauls covered a larger area also including the area southwest of Beer Island and off the north-eastern coast of Norway (Fig. 1). The water depth in the trawled areas varied between 75 and 390 m. Seabed sediment types were different mixtures of sand, mud, gravel, cobbles and boulders (Table 1).

A towed underwater vehicle (FOCUS 2, MacArtney AS) was deployed to make visual observations of the trawl and extension, measurements of cross-section from trawl opening to end of the last extension, and acoustic measurements of sediment plume height. Trawl cross-section and clearance above seabed were measured using a scanning sonar (Kongsberg Mesotech Ltd), with measurements taken at each panel seam. In this way, a simple diagram of the trawl's geometry and seabed clearance could be made. Sediment plume height was measured using a 200 kHz split beam echosounder affixed to the vehicle. The procedure for collecting and analysing the acoustic data is described in greater detail in Section 2.3. The towed vehicle can only be deployed in calm seas and the deployment and orienting to correct position require significant time. Therefore, it was only used in eight stations to measure trawl geometry and cross-section and in two stations to measure sediment plume height.

Standard trawl sensors were placed on the trawl to give point measurements of geometry on all hauls. A Simrad PX TrawlEye (Kongsberg Maritime AS), a wireless catch monitoring sensor with a built-in echo sounder, was attached to the upper panel of the extension 4 m from the end of the extension (Fig. 2). The echosounder measured both the extension's height above the seabed and the separation between the upper and lower panels of the extension. A second TrawlEye was mounted in the roof of the trawl opening, immediately above the footrope, to monitor opening height and seabed contact (visual monitoring of footrope and seabed in the echogram). Simrad PX door sensors measured door spread and angle to ensure that the trawl maintained proper opening geometry and the doors were on the seabed.

2.3. Acoustic measurements of sediment plume height

A Simrad wide band transceiver (WBT Tube) with a 200 kHz split-beam transducer (ES200–7CDK, Kongsberg Maritime AS) was affixed to the towed underwater vehicle and used to measure the sediment plume height. The vehicle was navigated along the trawl wires to the trawl opening and further back toward the codend using the video camera and scanning sonar. Once in position the vehicle was maneuvered slightly to the side of the trawl extension (to avoid acoustic shadowing from the Deep Vision and trawl net) and remained in position while acoustic data were collected. The echosounder was operated in continuous wave (CW) mode with 0.512 ms pulse duration and 1 Hz transmission rate. Acoustic data were collected in hauls 15 and 23 (Table 1) and processed in the Large-Scale Survey System, LSSS (Korneliussen et al., 2016). Volume backscattering strengths (S_v, dB re 1 m^{-1}) (Maclennan et al., 2002) as a function of ping and range were exported to R (R Core Team, 2022) for further analyses. Background noise levels were obtained by selecting a period where the towed vehicle was at similar distance to seabed, but with no effect of trawling. From these data, the median, 25th and 75th quantile S_v values over all pings and along beam samples were calculated in R. The 75th quantile was then used as the threshold to extract sediment plume echoes from background noise. The seabed was detected from the echograms using thresholding, and the distance from the seabed to the top of the sediment plume was measured for each ping. To avoid false detections, an 11-ping running-median filter was applied before further analyses.

2.4. Analyses of image clarity

Image clarity was analysed for GoPro video and Deep Vision images (camera type and number of images analysed are summarised in Table 1). To ensure that only images taken when the trawl was on the seabed, and the sediment plume generated by the ground gear would have reached the location of the camera, the first minute of each trawl station was excluded from analysis. This offset was determined by calculating the horizontal distance from the centre of the ground gear to the location of the camera divided by the average trawling speed (elapsed time on seabed divided by distance covered as recorded in the vessel's log). Depending on the arrangement of extra extension pieces (Table 1) and placement of cameras, the time offset was calculated to be 34–53 s. Image clarity score (scoring systems described below) was correlated to height above seabed as measured by the TrawlEye mounted adjacent to the camera system. Some of the hauls lacked data from the TrawlEye. In these hauls, the height was either obtained from measurements with the scanning sonar in the FOCUS vehicle (hauls 1 and 7) or the average height measured in hauls with the same rigging was used (hauls 11, 12 and 18). All TrawlEye measurements more than 15 m above seabed were regarded as outliers and removed.

2.4.1. GoPro images

The GoPro video files were replayed in VLC media player (VideoLAN Organization). The recordings were paused every 10 s, and the still images were viewed and scored. Two cameras were used, and it was discovered after the cruise that one collected video at a resolution of 1280 pixels w × 720 pixels h while the other collected at 1920 × 1080 pixels. Since the cameras were used to measure relative visibility rather than absolute resolution, we assumed that this had no effect on the analyses. The videos were enhanced by setting saturation to 0 (greyscale), and brightness and contrast to + 50%. Image clarity was scored using three categories; 3 - Unobstructed visibility (both top and under panels of the trawl extension are visible), 2 - Partially obstructed

Fig. 3. Example images showing the categories used for scoring GoPro images. 3: Unobstructed visibility (a), 2: Partially obstructed visibility (b) and 1: Fully obstructed visibility (c).

visibility (only top panel visible) and 1 - Fully obstructed visibility (cannot see any meshes) (Fig. 3). Between 118 and 738 images were evaluated in each of the five trawl hauls (Table 1).

2.4.2. Deep Vision images

The Deep Vision camera system was operated at maximum resolution (2465 × 2054 pixels), exposure = 1/1000 s, gain = 1.5, and gamma = 1. Images were exported using the Deep Vision Analysis software (version 3.3RC9) in colour-corrected and geometrically rectified format. Image clarity was visually assessed as quantified image resolution using an ISO 12233 camera resolution test chart. The test chart was printed at a size of 291 mm high × 520 mm wide and affixed to the background of the Deep Vision imaging chamber 870 mm from the cameras (Fig. 4). The resolution was determined by assessing the minimum line spacing which remained visible in the image. The chart includes a range of line spacing targets corresponding to 1/100 – 1/1000 of its height, translating to resolution of 2.91 mm (score = 1) to 0.291 mm (score = 10). The test chart covered the central ~30% of the field of view of the cameras and contained multiple locations where resolution could be assessed. When possible, resolution was measured on the portions of the chart near the center. One hundred images were randomly selected from each of the 17 hauls where the Deep Vision camera system was used (Table 1).

2.4.3. Statistical analyses

The statistical analyses were undertaken in R version 4.2.2 (R Core Team, 2022). Images collected with the GoPro and Deep Vision camera systems were analysed separately due to differences in camera systems and methods of evaluating image clarity. For the GoPro data the probability of obtaining clear images as a function of camera height above seabed was investigated using a binomial generalized linear mixed effects model (GLMM) with a logit link, library glmmTMB (Brooks et al., 2022). This required reducing the numeric scores of image clarity to binary categories “obstructed” and “unobstructed” views. GoPro scores of 1 (fully obstructed) and 2 (partly obstructed) were grouped “obstructed” and score 3 (unobstructed) rated “unobstructed” (Fig. 3). To account for between haul variation, haul number was included as a random factor in the model. The significance of height above seabed was investigated using a likelihood ratio test (LRT) (Chambers, 1992). Model assumptions were verified by examining residuals using the DHARMa package in R (Hartig, 2020). Results from Deep Vision image analyse were not statistically tested due to small variation in camera height above seabed and mainly clear images. The data were analysed by visually comparing mean resolution scores (with standard deviations)

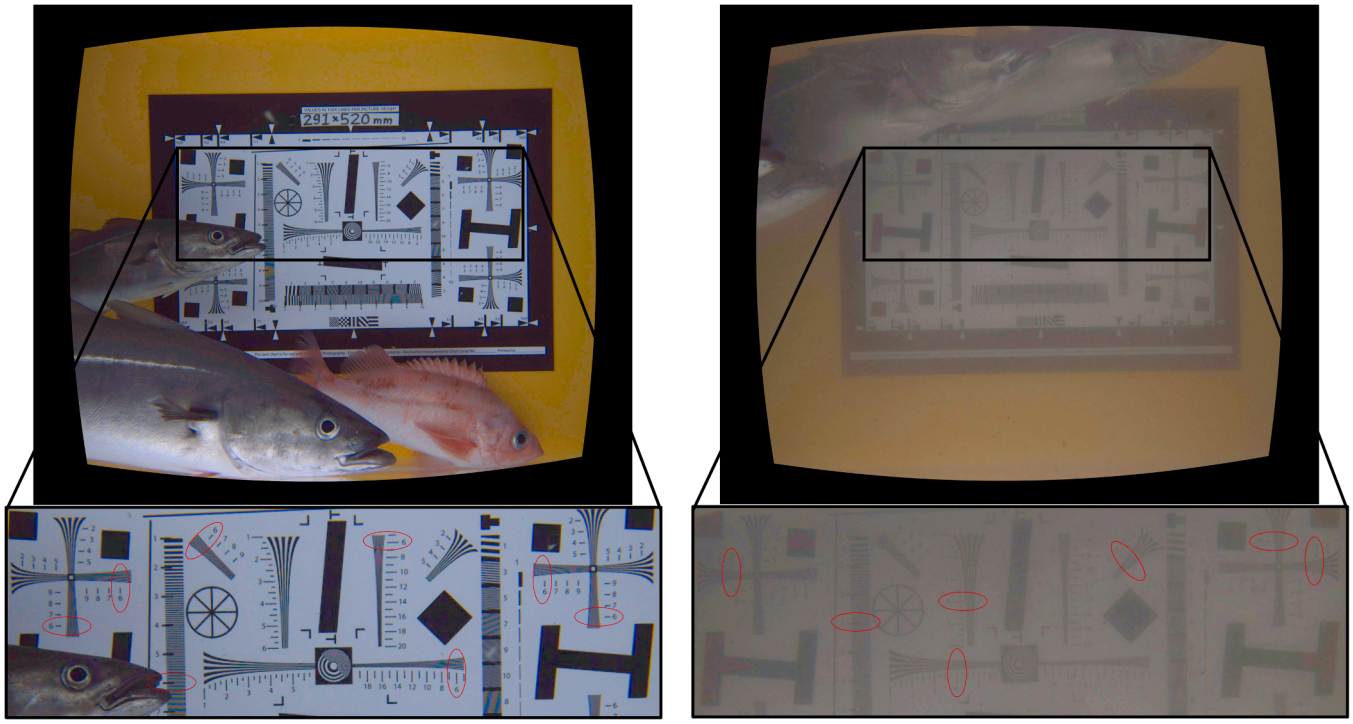

Fig. 4. Example images from the Deep Vision system showing ISO 12233 camera resolution test chart. In this instance, the minimum spacing where gaps between lines are visible is at a score of 6 in the left image (0.49 mm resolution) and 4 (0.73 mm resolution) in the right image. Passing fish are pollack (*Pollachius pollachius*) and redfish (*Sebastes* genus, not identified to species).

between hauls and in different sediment types.

3. Results

3.1. Acoustic measurements of sediment plume height

The acoustic measurements of sediment plume height made from the FOCUS underwater vehicle show that the median volume backscattering strength (S_v in dB) from the background (i.e., no trawl generated sediment plume) was − 78 dB (−85 and −70 dB for 25th and 75th quantiles respectively) (Fig. 5a). The 75th quantile (i.e., −70 dB) was used as the S_v threshold to extract sediment plume backscatter from the background. This resulted in an average sediment plume height of 5.1 m (SD 1.7 m) in haul 15 and 4.3 m (SD 1.7 m) in haul 23 (Fig. 5b and c).

3.2. Image clarity in GoPro

When the camera was 4 m above seabed (trawl hauls 1–3) visibility was unobstructed in 34%, partly obstructed in 52% and fully obstructed in 13% of the images. At 6 m above seabed (trawl haul 4) visibility was unobstructed in 65%, partly obstructed in 34% and fully obstructed in 1% of the images. At 11 m above seabed (trawl haul 5) visibility was unobstructed in 96%, partly obstructed in 4% and fully obstructed in none of the images. Based on the GLMM model results the probability of getting a clear image was significantly higher when camera height above seabed was increased from 4 to 11 m (df = 1, LRT = 8.156, p = 0.004) (Fig. 6).

3.3. Image clarity in Deep Vision

The Deep Vision camera system was on average between 9.2 and 10.5 m above seabed resulting in almost exclusively clear images. In all trawl hauls image clarity was scored 6 in 74–100% of the images and no images were scored below 3. Average image clarity scores between trawl hauls ranged from 5.69 to 6 (SD 0.0 – 0.58) with no clear relationship with sediment type (Fig. 7).

3.4. Performance of the modified trawl

The trawl was towed at a speed between 3 and 4 kts, similar to commercial fishing operations (Fig. 8a). Door spread varied between 100 and 120 m in most of the hauls, and the trawl vertical opening was mainly between 6 and 7 m (Fig. 8b and c). In the first eight hauls with

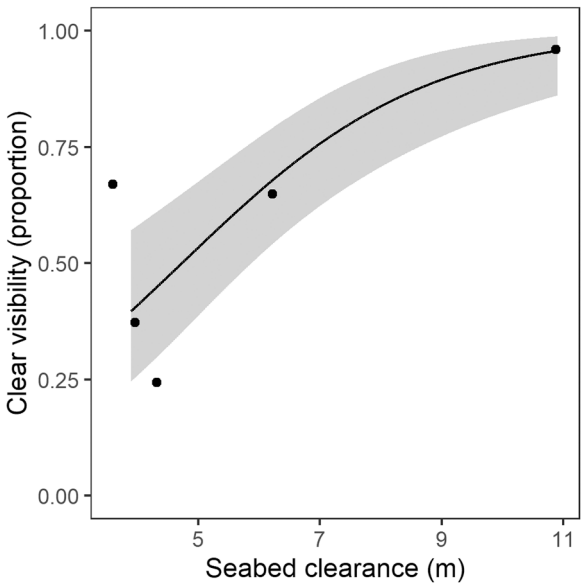

Fig. 6. Estimated probability (black line) with 95% confidence intervals (grey shaded area) of clear images at different heights above seabed. The black dots are the proportions of clear images in each haul. The camera system (GoPro) was attached in the extension of the demersal trawl.

rigging tests (Table 1) the codend clearance above seabed increased from 4 to 11 m (Fig. 8d). With the final rig (22 m long diamond mesh extension and 44 extra floats) codend clearance above the seabed was between 9.2 and 10.5 m (Table 1; Fig. 8d). There were no indications that the additional extensions and buoyancy reduced seabed contact. Measurements of the angle of the under panel in the bosom and extension sections of the trawl show that the increase in altitude and angle occurred only in the extensions (Table 2). The bottom panel of the trawl, from the footrope to the 2–4 panel transition (Fig. 2), maintained a 4° angle regardless of the of the configuration of the extra extensions. The under panel of the additional extensions increased from an angle of < 3° in the shorter configurations with 0–22 extra floats to 7–10° with longer extensions and 147–216 kg of added buoyancy. The rigid frame of the Deep Vision system kept the very end of the extension open, but video observations from the towed vehicle indicate that the extension ahead of the frame was not fully expanded. To test whether the water flow through the tunnel was affected, we tracked a passive floating object (a

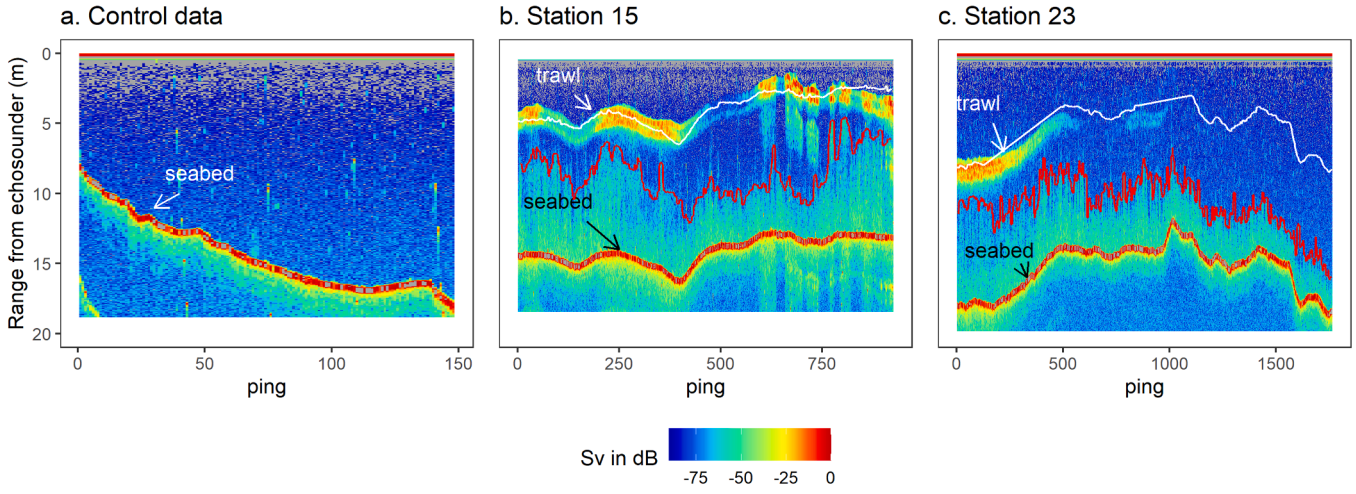

Fig. 5. Echograms based on acoustic data from the echosounder on the underwater vehicle. Panel a is the control data showing the seabed and no effect of trawling. Panels b and c show the seabed, trawl extension and sediment plume. The red line in panels b and c is the extracted sediment plume data and the white line is the extension height above seabed measured with a Simrad TrawlEye.

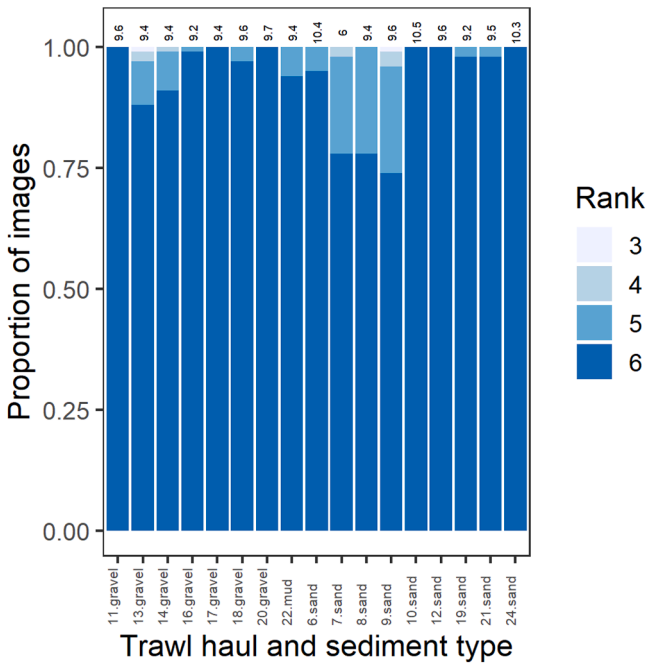

Fig. 7. Proportion of images by resolution score (3 was the lowest and 6 the highest scores registered). X-axis shows trawl haul number and main sediment type. The grain sizes were simplified to main categories: muddy, sandy and gravelly. The numbers on top of the columns are average camera heights (m) above seabed.

sea cucumber *Cucumaria frondosa*) for 9 consecutive Deep Vision images and calculated its speed. This gave en estimate of 1 knot water flow when trawling at 3 knots speed.

4. Discussion

This study shows that the sediment plume generated by a demersal trawl significantly reduces image clarity for in-trawl camera systems mounted in the trawl extension in the Barents Sea fishing grounds. The probability of getting clear images 4 – 6 m above the seabed was between 0.25 and 0.75, while at 10.9 m the probability increased to 0.95 (CI: 0.86 – 0.99). This limits the use of in-trawl camera systems unless proper measures are taken. To obtain clear images the camera system either needs to be lifted above the sediment plume, or the sediment plume must be prevented from entering the field of view of the camera.

Resuspended sediments by trawl doors and ground gear have been shown to reduce image clarity and contrast also in other studies, e.g., in the English ground fish survey (DeCelles et al., 2017), North Sea Norway lobster fishery (Sokolova et al., 2022) and in the Mediterranean Norway lobster areas (Fonseca et al., 2008). However, the size and concentration of the sediment plume will vary depending on sediment type, the type of trawl used and the hauling speed (O'Neill and Summerbell, 2011). In this study we measured the height of the sediment plume to 4 – 5 m using acoustic methods and the visibility was poor in 35% of the images at 6 m clearance from the seabed. In the North Sea, the sediment plume height 20 – 50 m behind the demersal otter trawl was measured to be 0.5 – 2 m high (Sokolova et al., 2022). This difference may be due to the larger ground gear and higher towing speeds used in our study compared to those in the *Nephrops* fishery (Sokolova et al., 2022). Our measurements were also made further behind the ground gear (80 m). Fishing activity in the area may also affect the amount of sediment in the water column following trawling. During our study we were the only vessel doing fishing operations in the area. However, during the peak fishing season, multiple boats often trawl actively in the same area and the sediment plume may be considerably higher and remain suspended for prolonged time (pers. communication Egil Skarbøvik, Skipper on FV "Ramoen"). In the Barents Sea fishing grounds, the sediment is mainly a mixture of mud, sand and gravel (Bøe et al., 2022). We did not detect a significant effect of grain size on image clarity, maybe due to relatively uniform sediments, too low resolution in grain size information or too low sample size.

We used a 200 kHz split-beam echosounder on an underwater vehicle to measure the height of the sediment plume. The echo sounder measurements of the relative position of the camera and the sediment plume effectively demonstrated the relationship between visibility and the plume. However, this is not an efficient method for routine use. It was not possible to detect the sediment plume in the echosounder data from the TrawlEye, but the option of using trawl mounted echosounders for more routine measurements could be considered. More accurate measurements of particle concentration and size behind trawl doors and ground gear have been made by O'Neill and Summerbell (2011) using a laser in-situ scattering and transmissometry (LISST 100X). Sokolova et al. (2022) used a turbidity meter attached to the trawl to measure how much occlusion the disturbed sediments caused at different locations in the trawl. O'Neill et al. (2013) compared acoustic (using multibeam sonar) and optic measurements of sediment concentration in plumes behind the otter door of a demersal trawl and behind the roller clump of a demersal twin trawl. They showed that accurate acoustic measurements can be obtained, but the accuracy is to some degree limited by the concentration and mean grain size. Information on grain size is also required for proper calibration of the acoustic system.

Fish have been observed to stop and accumulate in front of selection grids (Sistiaga et al., 2016) and in-trawl camera systems (Sokolova et al., 2022; Underwood et al., 2018). Fish accumulating ahead of the codend and then, when exhausted, entering in large densities may affect the efficiency of the selective devices and make image analyses less useful if not accounted for. In our study, there were indications that the water flow through the tunnel was reduced, and that the extension section was not fully expanded. Tapering from the last part of the trawl to the camera section may be a solution. Underwood et al. (2018) and DeCelles et al. (2017) showed that an in-trawl camera system attached to the extension of a tapered survey trawl performed well with no signs of collapse. However, this was not an option in our case due to the long extension and lack of sufficient meshes for tapering. Continuing the trawl's taper through an additional 22 m of extension was discussed with both net designers and commercial fishers but would have required significant modifications to the trawl, not feasible in this experiment. If efforts are made in the future to use additional extensions and buoyancy to raise the codend, work is necessary for ensuring proper water flow. One possible solution is the use of flexible kites to keep the extensions open, such as those used by Grimaldo et al. (2009).

As an alternative to raising the camera system above the sediment plume sediment suppressing sheets may be used. Sokolova et al. (2022) inserted a 3 m wide and 5 m long sediment suppressing sheet behind the ground gear and placed the camera unit in a four-panel tarpaulin section. This resulted in images that were clear enough to identify species during fishing with a camera system in the aft part of the trawl. This solution could be considered for the Barents Sea demersal trawl fisheries, but it is unknown whether it will be enough to suppress the sediment plume from the larger trawl and doors.

In our study the camera systems were mounted 80 m behind the ground gear in the tunnel where all the fish passing the camera can be monitored. If there is no need to monitor all fish entering the trawl and cover the whole area across, an option is to position the camera further up in the trawl, where it can be mounted higher above the seabed. This way the sediment plume may be less of an issue. However, using bright light closer to the trawl opening may disturb the behaviour of the fish.

In-trawl camera systems can contribute to more sustainable trawling. Trawling is the most efficient method for catching demersal fish accounting for about 30% of the total fisheries catch (Watson et al., 2006), and has an important role in meeting the increasing food demand in the

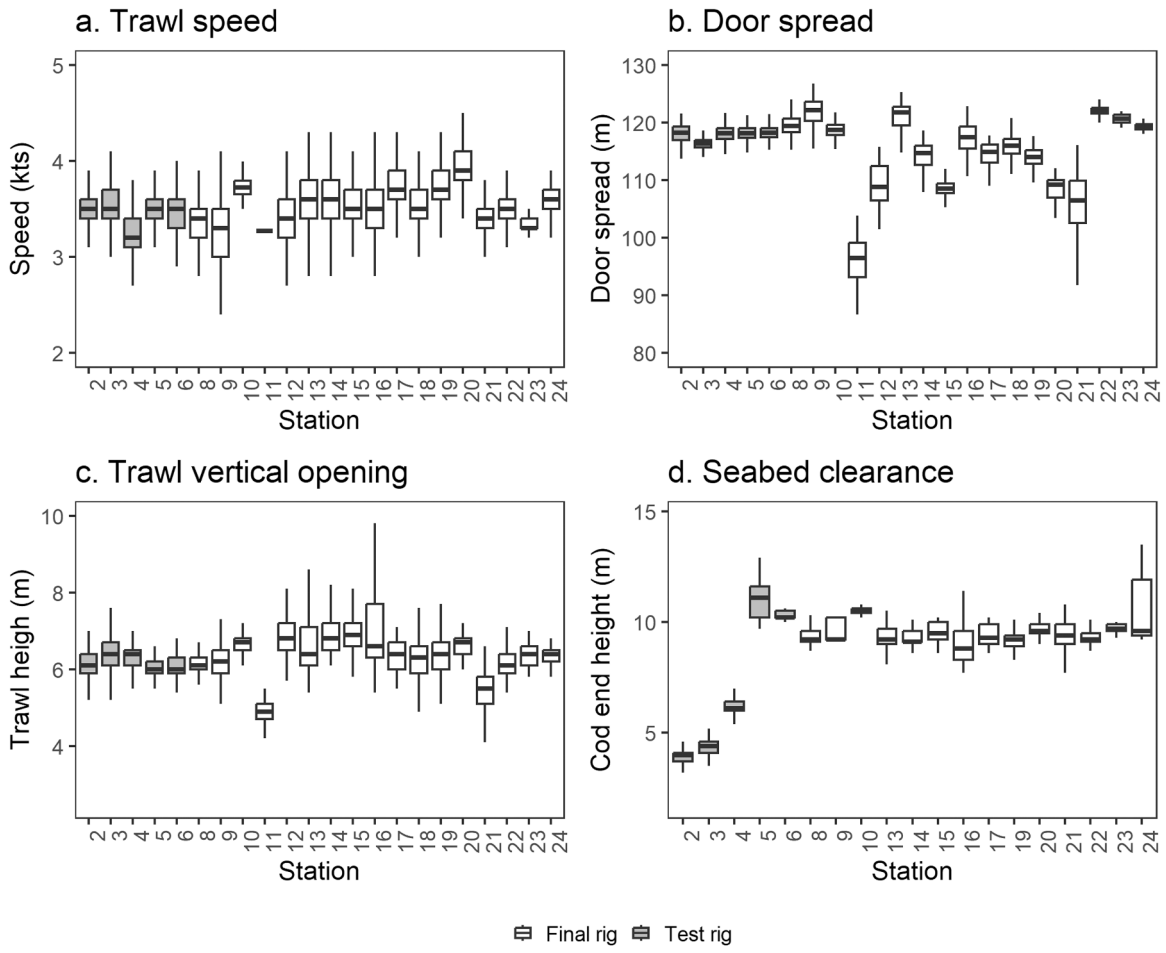

Fig. 8. Trawl speed over ground (a), door spread (b), trawl vertical opening (c) and codend / camera system height above seabed (d). Data were obtained from Simrad trawl sensors attached to the trawl doors, headline and extension. No data was available for hauls 1 and 7 and codend height data was also not available for hauls 11,12 and 18.

Table 2
Measurements of under panel angle from FOCUS towed vehicle under different extension configurations. In addition to the extensions, a 10.7 m long 2 – 4 panel transition piece was mounted at the end of the trawl. Under panel angle in "Extensions" includes this piece.

Haul No.	Length of extension (m)	Mesh type	Number floats	Under panel angle (deg) relative to seabed	
				Footrope to end of trawl	Extensions
2	10.7	diamond	0	3.7	0.3
3	15.0	square	0	3.8	2.7
4	15.0	square	22	4.1	2.2
5	37.0	square + diamond	44	4.1	7.1
6	37.0	square + diamond	44	4.2	8.8
7	22.0	diamond	30	3.7	7.1
8	22.0	diamond	44	4.2	9.9
9	22.0	diamond	44	4.5	8.0

World (FAO, 2022). However, demersal trawls may have negative impacts on the seabed and benthic organisms (Jørgensen et al., 2016; Kaiser et al., 2002) and have high fuel consumptions per kg fish landed (Sala et al., 2022). It is also the fishing method with highest by-catch rates (Pérez Roda et al., 2019). Therefore, there is a need to reduce the negative impacts of demersal trawling while maintaining the catch efficiency. Implementation of in-trawl cameras requires further development of practical solutions for reducing the sediment disturbance on images. This study shows that mainly clear in-trawl camera images can be obtained in the Barent sea demersal fishing grounds if the trawl is modified so that the extension with the camera system is raised 6 – 8 m above sea floor.

CRediT authorship contribution statement

Maria Tenningen: Conceptualization, Methodology, Formal analyses, Writing – Original Draft, Writing – Review & Editing, Project administration **Shale Rosen:** Conceptualization, Methodology, Formal analyses, Writing – Original Draft **E.H. Taraneh Westergerling**: Methodology, Formal analyses **Nils Olav Handegard:** Conceptualization, Writing – Original Draft, Writing – Review & Editing, Project administration, Funding acquisition.

Declaration of Competing Interest

The authors declare that they have no known competing financial interests or personal relationships that could have appeared to influence the work reported in this paper.

Data Availability

Data will be made available on request.

Acknowledgements

We would like to thank Arill Engås, Jostein Saltskår, Liz Kvalvik, Asbjørn Aasen and the crew on G.O. Sars for their assistance in designing and conducting the experiments, Erik Schuster and Sigurd Hannaas for operating the FOCUS underwater vehicle and Liz Kvalvik for creating drawings of the trawl and extensions. We would like to thank Neil Anders for advising us on statistical analyses. Staff at Selstad AS and Ramoen AS assisted in design and construction of the trawl extensions and staff at Scantrol Deep Vision AS and Girona Vision Research AS were helpful in designing the resolution experiments. The work was financed by the Research Council of Norway project "CRIMAC," grant number 309512.

References

Allken, V., Handegard, N.O., Rosen, S., Schreyeck, T., Mahiout, T., Malde, K., 2019. Fish species identification using a convolutional neural network trained on synthetic data. ICES J. Mar. Sci. 76, 342–349. https://doi.org/10.1093/icesjms/fsy147.

Allken, V., Rosen, S., Handegard, N.O., Malde, K., 2021. A deep learning-based method to identify and count pelagic and mesopelagic fishes from trawl camera images. ICES J. Mar. Sci. https://doi.org/10.1093/icesjms/fsab227.

Bøe, R., Bjarnadóttir, L.R., Elvenes, S., Dolan, M., Bellec, V., Thorsnes, T., Lepland, A., Longva, O., 2022. Revealing the secrets of Norway's seafloor – geological mapping within the MAREANO programme and in coastal areas. In: Geological Society, 505. Special Publications, London, pp. 57–69. https://doi.org/10.1144/SP505-2019-82.

Boldt, J.L., Williams, K., Rooper, C.N., Towler, R.H., Gauthier, S., 2018. Development of stereo camera methodologies to improve pelagic fish biomass estimates and inform ecosystem management in marine waters. Fish. Res. 198, 66–77. https://doi.org/10.1016/j.fishres.2017.10.013.

Bravata, N., Kelly, D., Eickholt, J., Bryan, J., Miehls, S., Zielinski, D., 2020. Applications of deep convolutional neural networks to predict length, circumference, and weight from mostly dewatered images of fish. Ecol. Evol. 10, 9313–9325. https://doi.org/10.1002/ece3.6618.

Brooks, M., Bolker, B., Kristensen, K., Maechler, M., Magnusson, A., McGillycuddy, M., Skaug, H., Nielsen, A., Berg, C., Bentham, K. van, Sadat, N., Lüdecke, D., Lenth, R., O'Brien, J., Geyer, C.J., Jagan, M., Wiernik, B., Stouffer, D.B., 2022. glmmTMB: Generalized Linear Mixed Models using Template Model Builder.

Chambers, J., 1992. 4. Linear Models, in: Statistical Models in S. Wadsworth and Brooks/Cole Advanced Books and Software, p. 608.

DeCelles, G.R., Keiley, E.F., Lowery, T.M., Calabrese, N.M., Stokesbury, K.D.E., 2017. Development of a video trawl survey system for New England groundfish. Trans. Am. Fish. Soc. 146, 462–477. https://doi.org/10.1080/00028487.2017.1282888.

Feyrer, F., Portz, D., Odum, D., Newman, K.B., Sommer, T., Contreras, D., Baxter, R., Slater, S.B., Sereno, D., Nieuwenhuyse, E.V., 2013. SmeltCam: underwater video codend for trawled nets with an application to the distribution of the imperiled delta smelt. PLOS ONE 8, e67829. https://doi.org/10.1371/journal.pone.0067829.

Fonseca, P., Correia, P.L., Campos, A., Lau, P.Y., Henriques, V., 2008. Fishery-independent estimation of benthic species density—a novel approach applied to Norway lobster Nephrops norvegicus. Mar. Ecol. Prog. Ser. 369, 267–271. https://doi.org/10.3354/meps07609.

Garcia, R., Prados, R., Quintana, J., Tempelaar, A., Gracias, N., Rosen, S., Vågstøl, H., Løvall, K., 2020. Automatic segmentation of fish using deep learning with application to fish size measurement. ICES J. Mar. Sci. 77, 1354–1366. https://doi.org/10.1093/icesjms/fsz186.

Graham, N., Jones, E.G., Reid, D.G., 2004. Review of technological advances for the study of fish behaviour in relation to demersal fishing trawls. ICES J. Mar. Sci. 61, 1036–1043. https://doi.org/10.1016/j.icesjms.2004.06.006.

Grimaldo, E., Larsen, R.B., Sistiaga, M., Madsen, N., Breen, M., 2009. Selectivity and escape percentages during three phases of the towing process for codends fitted with different selection systems. Fish. Res. 95, 198–205. https://doi.org/10.1016/j.fishres.2008.08.019.

Grimaldo, E., Sistiaga, M., Larsen, R.B., 2014. Development of catch control devices in the Barents Sea cod fishery. Fish. Res. 155, 122–126. https://doi.org/10.1016/j.fishres.2014.02.035.

Grimaldo, E., Sistiaga, M., Herrmann, B., Larsen, R.B., Brinkhof, J., Tatone, I., 2018. Improving release efficiency of cod (Gadus morhua) and haddock (Melanogrammus aeglefinus) in the Barents Sea demersal trawl fishery by stimulating escape behaviour. Can. J. Fish. Aquat. Sci. 75, 402–416. https://doi.org/10.1139/cjfas-2017-0002.

Gullestad, P., Blom, G., Bakke, G., Bogstad, B., 2015. The "discard ban package": experiences in efforts to improve the exploitation patterns in Norwegian fisheries. Mar. Policy 54, 1–9. https://doi.org/10.1016/j.marpol.2014.09.025.

Hartig, F., 2020. DHARMa: Residual Diagnostics for Hierarchical (Multi-Level / Mixed) Regression Models.

Jørgensen, L.L., Planque, B., Thangstad, T.H., Certain, G., 2016. Vulnerability of megabenthic species to trawling in the Barents Sea. ICES J. Mar. Sci. 73, i84–i97. https://doi.org/10.1093/icesjms/fsv107.

Kaiser, M.J., Collie, J.S., Hall, S.J., Jennings, S., Poiner, I.R., 2002. Modification of marine habitats by trawling activities: prognosis and solutions. Fish Fish 3, 114–136. https://doi.org/10.1046/j.1467-2979.2002.00079.x.

Kim, Y.-H., Wardle, C.S., 1998. Modelling the visual stimulus of towed fishing gear. Fish. Res. 34, 165–177. https://doi.org/10.1016/S0165-7836(97)00089-1.

Korneliussen, R.J., Heggelund, Y., Macaulay, G.J., Patel, D., Johnsen, E., Eliassen, I.K., 2016. Acoustic identification of marine species using a feature library. Methods Oceanogr. 17, 187–205. https://doi.org/10.1016/j.mio.2016.09.002.

Maclennan, D.N., Fernandes, P.G., Dalen, J., 2002. A consistent approach to definitions and symbols in fisheries acoustics. ICES J. Mar. Sci. 59, 365–369. https://doi.org/10.1006/jmsc.2001.1158.

Naseer, A., Baro, E.N., Khan, S.D., Vila, Y., 2022. A novel detection refinement technique for accurate identification of nephrops norvegicus burrows in underwater imagery. Sensors 22, 4441. https://doi.org/10.3390/s22124441.

O'Neill, F.G., Summerbell, K., 2011. The mobilisation of sediment by demersal otter trawls. Mar. Pollut. Bull. 62, 1088–1097. https://doi.org/10.1016/j.marpolbul.2011.01.038.

Pérez Roda, M.A., Gilman, E., Huntington, T., Kennelly, S.J., Suuronen, P., Chaloupka, M., Medley, P., 2019. third assessment of global marine fisheries discards. FAO Fisheries and Aquaculture Technical Paper (FAO) eng no. 633.

Rose, C.S., Barbee, D., 2022. Developing and testing a novel active-selection (ActSel) bycatch reduction device to quickly alternate trawls between capture and release configurations with real-time triggering. Fish. Res. 254, 106380 https://doi.org/10.1016/j.fishres.2022.106380.

Rosen, S., Holst, J.C., 2013. DeepVision in-trawl imaging: sampling the water column in four dimensions. Fish. Res. 148, 64–73. https://doi.org/10.1016/j.fishres.2013.08.002.

Sala, A., Damalas, D., Labanchi, L., Martinsohn, J., Moro, F., Sabatella, R., Notti, E., 2022. Energy audit and carbon footprint in trawl fisheries. Sci. Data 9, 428. https://doi.org/10.1038/s41597-022-01478-0.

Sistiaga, M., Herrmann, B., Grimaldo, E., Larsen, R.B., Tatone, I., 2015. Effect of lifting the sweeps on bottom trawling catch efficiency: a study based on the Northeast arctic cod (Gadus morhua) trawl fishery. Fish. Res. 167, 164–173. https://doi.org/10.1016/j.fishres.2015.01.015.

Sistiaga, M., Brinkhof, J., Herrmann, B., Grimaldo, E., Langård, L., Lilleng, D., 2016. Size selective performance of two flexible sorting grid designs in the Northeast Arctic cod (Gadus morhua) and haddock (Melanogrammus aeglefinus) fishery. Fish. Res. 183, 340–351. https://doi.org/10.1016/j.fishres.2016.06.022.

Sokolova, M., Mompó Alepuz, A., Thompson, F., Mariani, P., Galeazzi, R., Krag, L.A., 2021a. A deep learning approach to assist sustainability of demersal trawling operations. Sustainability 13, 12362. https://doi.org/10.3390/su132212362.

Sokolova, M., Thompson, F., Mariani, P., Krag, L.A., 2021b. Towards sustainable demersal fisheries: NepCon image acquisition system for automatic Nephrops norvegicus detection. PLoS One 16, e0252824. https://doi.org/10.1371/journal.pone.0252824.

Sokolova, M., O'Neill, F.G., Savina, E., Krag, L.A., 2022. Test and development of a sediment suppressing system for catch monitoring in demersal trawls. Fish. Res. 251, 106323 https://doi.org/10.1016/j.fishres.2022.106323.

Stokesbury, K.D.E., Cadrin, S.X., Calabrese, N., Keiley, E., Lowery, T.M., Rothschild, B.J., DeCelles, G.R., 2017. Towards an improved system for sampling new england groundfish using video technology. Fisheries 42, 432–439. https://doi.org/10.1080/03632415.2017.1342630.

Underwood, M.J., Rosen, S., Engås, A., Eriksen, E., 2014. Deep Vision: an In-Trawl stereo camera makes a step forward in monitoring the pelagic community. PLOS ONE 9, e112304. https://doi.org/10.1371/journal.pone.0112304.

Underwood, M.J., Rosen, S., Engås, A., Jørgensen, T., Fernö, A., 2018. Species-specific residence times in the aft part of a pelagic survey trawl: implications for inference of pre-capture spatial distribution using the Deep Vision system. ICES J. Mar. Sci. 75, 1393–1404. https://doi.org/10.1093/icesjms/fsx233.

Urquhart, G.G., Stewart, P., 1993. A review of techniques for the observation of fish behaviour in the sea.

Watson, R., Revenga, C., Kura, Y., 2006. Fishing gear associated with global marine catches: I. Database development. Fish. Res. 79, 97–102. https://doi.org/10.1016/j.fishres.2006.01.010.

Williams, K., Wilson, C.D., Horne, J.K., 2013. Walleye pollock (Theragra chalcogramma) behavior in midwater trawls. Fish. Res. 143, 109–118. https://doi.org/10.1016/j.fishres.2013.01.016.

Winger, P.D., Eayrs, S., Glass, C.W., 2010. Fish Behavior near Bottom Trawls. Behavior of Marine Fishes. John Wiley & Sons, Ltd, pp. 65–103. https://doi.org/10.1002/9780813810966.ch4.